A Configuration for Re-Entry from Mars Missions Using Aerobraking

D. J. SHAPLAND,* D. A. PRICE,† AND L. F. HEARNE‡
Lockheed Missiles and Space Company, Sunnyvale, Calif.

A new concept in re-entry vehicle configuration is proposed which results in a family of compact shapes with lift-to-drag (L/D) ratios of 0.5 to 1.0. The main heat shield consists of a circular cone raked off at an angle to provide sufficient lifting surface. The afterbody is an elliptical cone fitted to the cross section of the forecone. Trim at zero angle of attack results in a symmetrical flow field over the forebody which makes the shape amenable to reliable analysis. Re-entry criteria are evaluated in terms of aerodynamic and guidance requirements for speeds up to 65,000 fps. These criteria are satisfied with an L/D value as low as 0.6 if a closed-loop re-entry guidance system is used. Operational trajectories are described, and sufficient corridor and range maneuverability is demonstrated using trimmed lift roll control. A detailed analysis of the radiative and convective heating shows that ablation heat-protection methods are adequate. Important factors affecting the heat transfer are radiation loss from the airstream, mass transpiration effects on the boundary layer, and shock-layer vorticity. For re-entry at 65,000 fps, the heat-shield weight for a six man vehicle is about one-third of the total vehicle weight.

Nomenclature

A = reference area
C_D = drag coefficient
C_L = lift coefficient
D = drag force
G = normalized acceleration
l = characteristic length
L = lift force
r_N = nose radius
r_B = radius of base reference area
Re_t = transition Reynolds number
s = distance from stagnation point (along body contour)
V_E = re-entry velocity
W = weight
y = distance from stagnation point (normal to body)
α = angle of attack
γ_E = re-entry angle
δ = cone rake (slice) angle or shock-layer thickness
θ = sweepback angle
$\Delta\theta$ = range angle
ϕ = roll angle
ϕ_{II} = re-entry roll angle
ϕ_{IV} = final descent roll angle

Introduction

A RECENT study[1] developed a preliminary design of an Earth re-entry vehicle for use at the termination of a manned Mars mission departing Earth in the period 1971–1975. The results of the flight mechanics and thermodynamics analyses are reported in this paper. Details of specific missions were provided by NASA in which the associated re-entry speeds range from 45,000 to 65,000 fps. The available re-entry corridor width depends on the approach speed and aerodynamic characteristics of the vehicle. Thus, a configuration must be developed that minimizes the heat transfer and whose aerodynamics are compatible with the requirements set by the approach guidance accuracy. State-of-the-art materials and subsystems were assumed for the study.

Presented as Preprint 64-480 at the 1st AIAA Annual Meeting, Washington, D. C., June 29–July 2, 1964; revision received November 19, 1964. This research was sponsored by the NASA Manned Spacecraft Center, Houston, Texas.

* Senior Advanced Systems Engineer. Member AIAA.
† Staff Scientist.
‡ Research Specialist.

Re-Entry Criteria

The general influence of re-entry mode, velocity, and vehicle aerodynamic characteristics on entry system configuration has been discussed by Love.[2] The configuration proposed here uses the roll mode for extra-atmospheric orientation and for control within the atmosphere. Since the vehicle trims at zero angle of attack, roll maneuvers are easily performed using a reaction control system. A typical re-entry trajectory has the following characteristics. About half an hour before re-entry, the final velocity change is made by means of the main mission module propulsion, and the re-entry module separates from the spacecraft. This correction must be accurate enough to enable the re-entry vehicle to attain the re-entry corridor. The undershoot boundary is limited by the 10-G deceleration tolerance limit of the crew. The vehicle pulls out around 200,000 ft; at this point, maximum deceleration and heating are encountered. A period of constant altitude deceleration follows, during which negative lift is used to keep the vehicle within the atmosphere. When the roll angle ϕ has been reduced to zero, an equilibrium glide path is maintained. If ϕ is held at some value between 0° and 90°, greater cross range may be obtained. A skip maneuver may be initiated to increase down range; in this case, a second re-entry occurs for which the heating and decleration forces are much less severe than during initial pull-out. Conventional parachute recovery is assumed.

Using this re-entry concept, aerodynamic requirements were established and are shown in Fig. 1. The results are for a nonrotating spherical Earth with an instantaneous roll maneuver at pull-out. The effect of W/C_LA is slight. For a 65,000 fps re-entry speed, increasing the L/D value from 0.6 to 1.0 only increases the corridor width by about 2.5 naut miles. The available corridor width is, therefore, limited to about 11 naut miles (L/D = 1.0) for the upper speed value. If the acceleration limit on the lower boundary can be increased, the corridor can be widened approximately 1 naut mile/G. Lift modulation can be used to achieve slightly increased corridor width.[2,3] However, this maneuver changes the location of the stagnation point and destroys the flow-field symmetry of the concept discussed here. Approach guidance considerations, using a model suggested by Breakwell,[4] showed that a final trajectory correction about 20 min before re-entry (at 65,000 fps) will give a 3σ probability of achieving a 10-naut-mile corridor if the instrument uncertainty does not exceed 25 arc-sec.

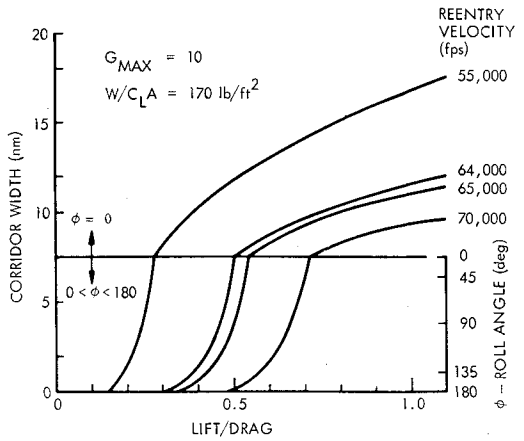

Fig. 1 Re-entry aerodynamic requirements.

The available landing area depends on the maneuver capability of the re-entry vehicle. That portion of the Earth's surface that can be reached depends on the re-entry point, the minimum direct re-entry range, and the skip range increment. The inclination of the approach orbit can be adjusted by a small velocity increment far from Earth. Thus, the landing point control pattern can be rotated around the central asymptote. The resulting spherical Earth patterns for two re-entry velocities (nonoptimum) associated with a 1973 opposition mission are shown in Fig. 2; $\Delta\theta$ represents the range angle for the 45,000 fps case measured from the asymptote. The results are for an L/D ratio of 0.5, the lowest value considered in the study. In both cases, a skip range increment of 10,000 naut miles was assumed. The asymptote declination varies between $-20°$ and $+8°$ for the missions under consideration. Thus, landing sites in opposite hemispheres (e.g., Edwards or Woomera) will have a landing window of about 14 and 16 hr, respectively. An appropriate midcourse correction can be used to adjust the arrival time if necessary. Because of the flexibility of the orbit inclination change technique available during the trans-Earth phase, only lateral range maneuvers sufficient to account for approach-guidance errors are required.

Vehicle Selection

At the re-entry speeds involved in return from a Mars mission, radiation heat transfer will be of major importance. From this point of view, a very blunt shape is undesirable. However, convective heating cannot be ignored, and convective heating rates are reduced by increasing the bluntness. A compromise must be made. This indicates a conical shape with a relatively small nose radius that retains a degree of over-all bluntness that is consistent with lifting requirements. Cone angle is, therefore, an important parameter and must be optimized. Radiative heating increases with increasing cone angle (low W/C_LA), whereas small cone angles imply high W/C_LA values and deceleration at relatively low altitude where convective heating may predominate.

The re-entry corridor width is strongly influenced by the allowable G tolerance level. Thus, the crew must be placed so that the resultant deceleration force acts in the direction that provides the highest tolerance level. This is the "eyeballs-in" position indicated in Fig. 3a. Utilization of lift to ameliorate acceleration and guidance requirements and provide range maneuverability determines the orientation of the human occupant with respect to the flight direction as shown in Fig. 3b. The occupant establishes a minimum characteristic dimension l for the vehicle. Crew number and orientation defines a minimum frontal area (Fig. 3c). To insure aerodynamic stability, the forward surface must be shaped to provide a center of pressure sufficiently far aft to provide trim and to yield an adequate stability margin for desirable center-of-gravity location (Fig. 3d). The forward surface must also be shaped to provide the best compromise for heating environment. Whereas the crew orientation is set by the lifting requirement, the vehicle attitude and nose shape are subject to design optimization.

To develop configuration concepts and define re-entry system requirements, a reference re-entry configuration was defined.[5] As shown in Fig. 4, the reference configuration consists of portions of two cones. The forebody (main heat shield) is a spherically blunted circular cone raked off at some angle δ to yield the desired L/D value. The afterbody is a right elliptic cone fitted to the elliptic cross section of the forebody cone. The size of the vehicle is established in terms of the characteristic dimension and volume requirements. The configuration is made amenable to flow-field analyses by insuring trim at zero angle of attack (relative to the forecone centerline). This condition requires center-of-gravity offset as shown in the figure. Variation of geometrical factors, such as nose radius, forecone angle, base area, rake angle, and afterbody shape, produces a whole family of vehicles. The L/D values for this family range from 0.5 to 1.0, so that the reference configuration provides reliable data for comparison with other configurations and concepts. Detailed analyses of performance and subsystem design were based on a configuration with an L/D value of 0.6, a half-cone angle of 35°, a volume of 500 ft^3, and a drag parameter of 204 lb/ft^2. Most of the results on operational performance and heat-shield design given later are for this vehicle re-entering at 65,000 fps. However, the analyses developed and the results obtained are applicable to any project concerned with Earth re-entry at hyperbolic speeds.

Configuration Aerodynamics

Operating the reference configuration at zero angle of attack makes possible a reliable prediction of the aerodynamic characteristics which is based on conical flow solutions and verified by extensive wind-tunnel tests. The basic assumption is that the whole surface is exposed to the flow, i.e., the Mach lines from the corners of the slice do not intersect the forecone surface. For the range of geometry of interest and high Mach numbers encountered during the re-entry, this is indeed the case. Furthermore, the simple Newtonian impact theory predicts these aerodynamic characteristics with sufficient accuracy for the purposes of preliminary design studies. Therefore, only "pure" Newtonian (pressure coefficient of 2) flow was used to calculate the hypersonic aerodynamic characteristics for both trim at zero angle of attack and untrimmed conditions including sideslip.

Large variations in the trim aerodynamic characteristics can be obtained for the conical reference configuration family, as demonstrated in Fig. 5. With large cone angles, the aerodynamic characteristics are influenced only slightly by nose-bluntness ratios between 0 and 0.4. With greater sweepback, the nose bluntness produces a significantly greater effect, as is indicated by the $\theta = 60°$ curves. The L/D value at zero angle of attack is set primarily by the

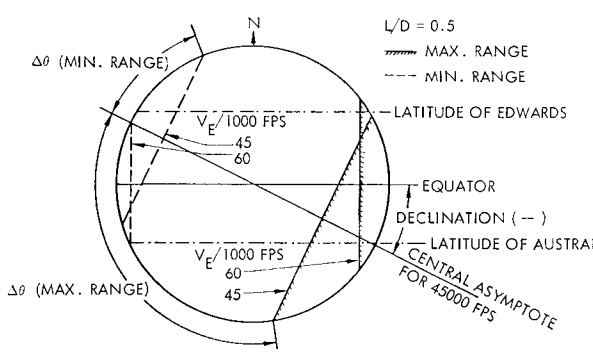

Fig. 2 Earth landing coverage.

choice of the slice angle δ. For zero nose radius the aerodynamic characteristics are those for a flat plate at $\alpha = \delta$. The reference configuration family can provide aerodynamic characteristics representative of a wide variety of shapes such as the Langley Research Center HL-10 vehicle, or the M-2 vehicle developed at the Ames Research Center, or the Apollo configuration. The comparable trim conditions of the reference configuration to provide similar characteristics to these vehicles are indicated in Fig. 5 for the maximum lift conditions of the cited vehicles. Because the configuration so nearly represents flat-plate characteristics at an angle of attack near δ, the trim center-of-gravity position will be located essentially along the normal from the centroid of the slice area. Hence, the approximate center-of-gravity loci may be easily visualized for any member of the configuration family.

Center-of-gravity tolerance, ablation weight loss, and reaction system fuel expenditure will cause variations in the desired trim condition (i.e., zero angle of attack). The reference configuration exhibits small variations in the aerodynamic characteristics for small changes about the nominal angle of attack. For example, with 45° sweepback, a 30% decrease in L/D occurs, almost entirely due to the increase in drag coefficient with increasing angle of attack. The lift coefficient varies less than 10% from $-5°$ to 15° angle of attack with the peak values near 5°. Hence, the vehicle is operating near maximum C_L. Furthermore, the center of pressure undergoes relatively little change. The effect of sideslip is neglible on all quantities except drag coefficient, for which less than 10% deviation occurs. The lateral static stability is adequate for the smaller sweepback forecone angles. For example, with $\theta = 45°$, the stability aft limit is about midway between the slice plane and aft limit for the longitudinal static stability. Higher sweepback shapes impose more stringent center-of-gravity requirements for satisfactory lateral stability.

Operation at the minimum W/C_DA (or minimum W/C_LA at constant L/D) is desirable to reduce the magnitude of the heat load imposed upon the vehicle. However, minimum lift loading is limited for fixed weight and volume. The value of W/C_LA depends upon cone sweepback angle. Families representing constant L/D configurations reach a minimum value of W/C_LA which corresponds to the value for a flat plate at an angle of attack of θ. The L/D of 0.6 shape approaches the flat-plate minimum W/C_LA of 160 lb/ft²; this represents flat-plate operation at maximum C_L near 35° angle of attack. Although it is desirable to reduce W/C_LA as much as possible, considerations such as internal arrangement pose practical limits to both ends of the sweepback angle spectrum for the reference configuration family. One such aspect is the effect of geometry changes of the forebody cone on packaging efficiency because of the variation of the base-area geometry. Small sweepback angles cause a somewhat narrow base plan form (especially at higher L/D) and decrease the usable space.

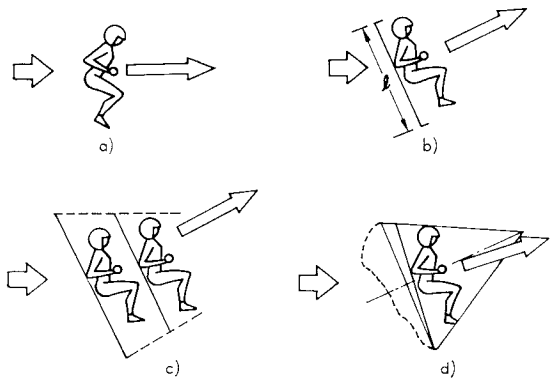

Fig. 3 Implications of crew orientation on configuration concepts.

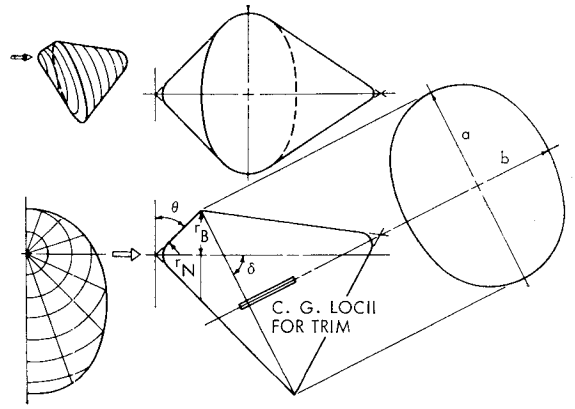

Fig. 4 Reference configuration geometry.

At the other end of the spectrum of sweepback angles, volume within the forecone displaces the more efficient aft cone space. The configuration approaches the slender shapes typified by the M-2 or HL-10 at small angles of attack. Thus, the reference-configuration family is seen to be representative of a wide range of re-entry-vehicle shapes of an apparently different geometry. Another geometrical property that will be important in minimizing heat-shield weight is the forecone surface area. A large increase of the lateral area occurs for larger sweepback angles at low L/D. Considerably lower forecone area for $L/D = 1$ implies the possibility of small heat-shield weight penalties due to increased L/D effects.

Re-Entry Flight Mechanics

As previously noted, the available aerodynamic corridor for the re-entry range of interest, illustrated in Fig. 1 for a typical W/C_LA value, is essentially a function of the L/D capability. The necessity of knowing position within the corridor is evident from the pull-out roll-angle scale. An L/D of 0.6 was selected for the nominal design point. The influence of finite roll rates on corridor control was examined. Minimum roll rates of 40°/sec were found to be sufficient to reduce corridor width degradation to within acceptable tolerance. Lift-loading variations considered in the study cause a maximum increase in corridor width of about 1.5 naut miles above those shown in Fig. 1.

Nominal Design Trajectories

Three discrete Earth re-entry trajectories were selected for vehicle design studies and are defined by direct re-entry along the upper and lower boundaries and by a maximum range skip from the upper-boundary trajectory. The upper boundary is defined for re-entry with constant maximum negative lift (180° roll angle) that yields pull-out at the altitude lift limit. The lower boundary is established for a 10-G maximum resultant acceleration prior to pull-out for any value of roll angle. The skip trajectory is determined for maximum lift capability (zero roll angle) with maneuvering delayed until

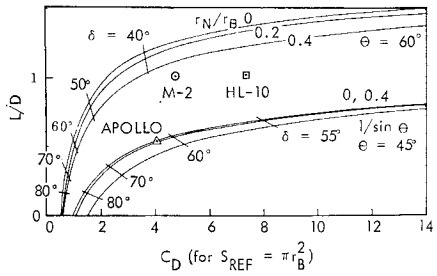

Fig. 5 Trim characteristics for $\alpha = 0$.

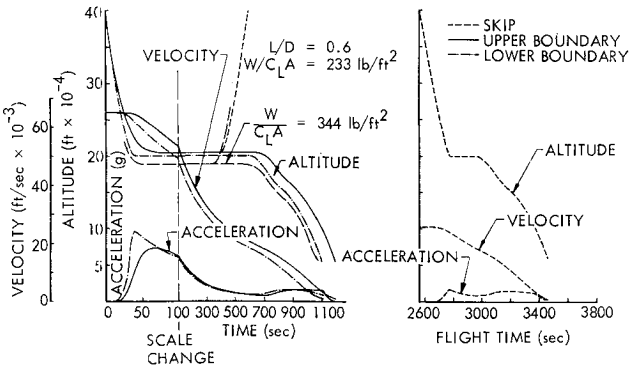

Fig. 6 Nominal design trajectory.

well below escape speed. The second re-entry from the skip trajectory follows the nominal trajectory model that utilizes positive lift (zero roll angle) only during the pull-out phase. Many variations of these nominal trajectory profiles are possible within the altitude velocity limits defined by the maximum acceleration and lift limit contours. However, the selected nominal trajectories provide representative re-entry performance for the maneuvering capability, heating and acceleration environment, and guidance requirements.

The altitude, velocity, and resultant acceleration histories for the three nominal design trajectories are presented in Fig. 6. Note the time-scale change soon after pull-out between 40–80 sec after re-entry. A small altitude difference (~4000 ft) between the upper-and lower-boundary trajectories is evident. The maximum resultant acceleration is high throughout the corridor (7–10 G), whereas the level for the second re-entry flight time is low because of the shallow path angle (2.4°). The second re-entry flight time is comparable to that for direct re-entry from 65,000 fps. The time interval above 400,000-ft alt is about 30 min for the 10,000 naut-mile skip. The apogee altitude of 150 naut miles is well under the radiation belt limit.

A change in the lift parameter affects only the operating altitude and flight time, as indicated for re-entry along the upper boundary with a W/C_LA of 344 lb/ft². The velocity and acceleration histories are essentially unaffected by the change in vehicle geometry. The second re-entry histories will be changed slightly because of the steeper flight path required for the 10,000-naut-mile skip when maneuvering from a lower operating altitude. The pull-out altitude is restricted to a band about 50,000-ft thick near 200,000 ft for the practical range of lift parameter examined during the study. The L/D characteristics causes only minor altitude variations along the upper boundary. The change in altitude of about 4000 ft across the corridor for an L/D of 0.5 is about doubled for an L/D of 1.0.

Range Maneuver Capability

The normal roll programing to maintain constant altitude yields a maneuver capability for direct re-entry that is more than adequate to account for cross-range deviations resulting from approach-guidance errors. This is illustrated in Fig. 7, where the familiar footprint is depicted for three positions within the corridor. The terminal trajectory trace for a final nominal descent roll angle (ϕ_{IV}) of zero degrees is shown for the upper boundary. Descent with a different constant roll angle yields the additional cross- and down-range combinations shown by the contour connecting the circled points. This incremental pattern applies to the other operating altitudes as well. Cross-range variations of about 1000 naut miles can be handled with the nominal trajectory profile by adjusting the operating altitude. Smaller cross-range maneuvers can be achieved by alternating the direction of the roll during the normal programing to control the trajectory heading appropriately. Down-range variations of about 1000 naut miles can be obtained by descent with a roll angle of 90°. The difference in down range between upper and lower boundary is increased only slightly (~120 naut miles) due to the shift of the re-entry point.

Variations of the lift parameter produce only minor changes in the maneuver capability, as indicated by comparison of the square and circle points for the lower boundary. The cross-range maneuver capability for the second re-entry is about one-fifth that for direct re-entry. The down-range capability is about the same over the variation of operating altitude that results from maximum range skip manuevers throughout the corridor. These results demonstrate adequate landing point control to account for guidance errors accumulated during the initial re-entry and skip maneuver. The cross-range capability during the first re-entry is utilized to supplement orbit inclination change to achieve the proper heading prior to the skip maneuver.

Roll-Control Mode

The trimmed lift roll-control mode was selected for the study to maintain a symmetrical flow field over the forecone and to avoid both the large reaction control fuel expenditure for pitch control and the design difficulties inherent in aerodynamic controls. Trim changes resulting from center-of-gravity variations with ablation and fuel expenditure and from shape changes are handled by a combination of internal mass balancing and reaction controls.

For practical vehicle shapes with mass distribution for trim at zero angle of attack, the principal axis will not coincide with the roll axis. This situation will require the application of a constant pitching moment during the roll maneuver in addition to the roll impulses to start and stop the motion. The pitching-moment fuel requirement is a relatively small portion of the total fuel requirement for compact shapes; for equal moments of inertia, the pitch requirement is eliminated. In addition, the total fuel requirements for the roll maneuvers at pull-out and skip are small as compared to the static roll trim requirement for lateral center-of-gravity errors. For example, with a vehicle pitch moment of inertia of 20,000 slug-ft², a fuel weight of only 10 lb is needed for each roll maneuver. A brief analysis of an on-off control technique indicated that, with proper control-system design, no significant increase in reaction fuel above the static roll trim requirements is needed. The attitude control system (fuel, nozzles, balancing fluid, and associated hardware) weighs about 10% of the total vehicle weight.

Re-Entry Guidance Concepts

The necessity for utilization of the roll-angle capability of the re-entry vehicle to provide a corridor also sets up stringent re-entry guidance requirements. This observation is supported by the open-loop guidance requirements presented in Fig. 8. The flight-path angle and roll-angle tolerances were determined for various corridor widths (obtained from approach

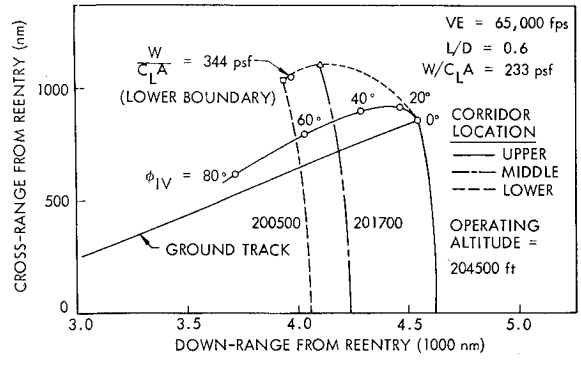

Fig. 7 Maneuver capability for direct re-entry.

guidance) as measured from the zero roll position. The minimum corridor boundary represents the difference between the zero roll angle and G (maximum) corridor positions for a given roll-angle tolerance. The requirements are obviously beyond the present state of the art. Hence, closed-loop guidance will be required during the initial re-entry phase. A brief examination of the acceleration profiles for various positions within the corridor indicated distinctive signatures that should be useful for this purpose.

Operational Performance

To demonstrate the ability of the re-entry system design to satisfy the operational constraints for the Mars mission, an exact Mars to Earth transfer trajectory was calculated for the 1975 opposition.

The final Earth approach phase is presented for the 1975 mission returning on November 11, 1976, with a re-entry speed of 65,000 ft-sec at an inclination of about 30°. The Moon is in good position for distance determination and exerts little nonlinear effects on the approach hyperbola.

The distinctive feature of the trajectory is its rectilinear character. The ground track for the typical Mars mission approach (from 12 hr) and re-entry trajectory is depicted in Fig. 9. The approach orbit inclination and declination are seen to be suitable for landing at Edwards Air Force Base (EAFB) without resort to midcourse guidance corrections. The departing hyperbola for no atmosphere is indicated by the dashed line. Re-entry occurs at about longitude 90°E just prior to vacuum perigee. The direct re-entry range capability indicates impact in the Philippine Sea or in New Guinea, where no prepared sites exist. Hence, either altitude maneuvering or a short skip to extend the trajectory to the EAFB site will be required. The inital re-entry is utilized to refine the midcourse orbit inclination selection to place the second re-entry trajectory track through EAFB. The direct re-entry range capability is insufficient to attain the Woomera site even with an appropriate orbit inclination change. The complete re-entry pattern rotates around the declination subpoint indicated by the small triangle. The direct re-entry "footprint" is still located in the Pacific Ocean, so that a short skip is required to reach Woomera.

The large mass changes resulting from ablation of the heat shield and expenditure of control-system fuel will alter these operational trajectories only slightly. The principal effect will be to reduce the direct re-entry range capability by about 20 naut miles cross range and 300 naut miles down range. Thus, no critical operational problems are anticipated with the re-entry system preliminary design as presented here.

Re-Entry Heating

A detailed investigation of the thermal environment encountered during atmospheric re-entry was conducted to establish heat-shielding requirements for the re-entry vehicle. A brief review of the significant phenomena, methods of analysis, and principal results is given in the succeeding sections. A comprehensive description of the analysis techniques that were employed has been given elsewhere.[6]

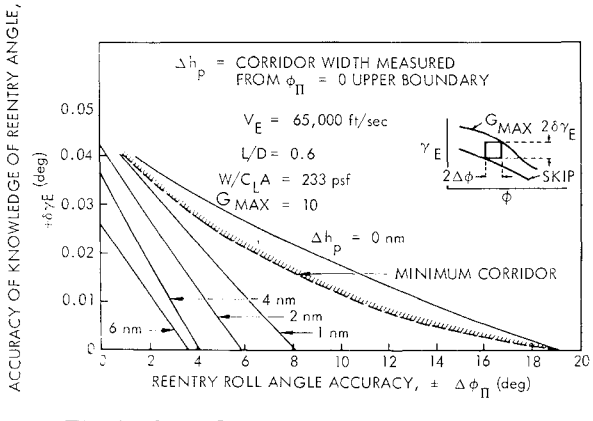

Fig. 8 Open-loop guidance requirements.

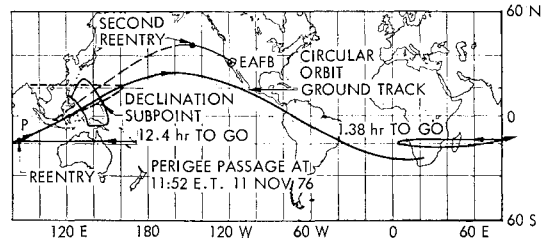

Fig. 9 Earth return trajectory (1975 opposition).

Aerothermal Environment

For re-entry at 65,000 fps, the thermal energy of the stagnated air at the vehicle tip exceeds 80,000 Btu/lb at early times in the trajectory. Stagnation pressures range up to about 2 atm. The conditions are such as to effect intense radiative emission from the gas as it flows over the vehicle, and consequently a realistic description of air emissivity is vital in the evaluation of the vehicle environment.

Theoretical results for the emissivity of air are in poor agreement, and insufficient experimental data are available to afford an assessment. A critical review of the available emissivity calculations was therefore undertaken[7] and resulted in adoption of an upper-bound model that is a composite of the results of Nardone, Breene et al.,[8] and Armstrong et al.[9]

Hypersonic approximations have been used to define the shock configuration and surface-pressure distribution for the forecone. The variation of flow conditions within the shock layer has been determined by solution of the conservation equations using the natural (streamline) coordinate system. The shock is tightly wrapped about the body. Pressure variation through the shock layer in a direction normal to the surface is small. Vorticity induced in the flow over the cone by the curved bow shock is appreciable; i.e., large velocity and density gradients exist normal to the body surface. The velocity and density both increase by about a factor of 2 through the vortical layer. However, at positions relatively far removed from the nose ($s/r_N > 10$), thickness of the vortical layer is small, and the shock-layer flow essentially corresponds to that for a pure cone.

Convective Heat Transfer

The basic methods used in the calculation of convective heating are conventional ones.[10–12] The boundary layer is assumed to transit from laminar to turbulent at a local Reynolds number value of 2×10^5. This criterion was adopted after review of data acquired in ballistic missile development flight tests and research vehicle flight tests. With this criterion, the boundary layer is turbulent over most of the vehicle surface during the period of high heat fluxes.

The convective heating level on the cone depends on the thickness of the boundary layer relative to that of the vortical layer. A very thin boundary layer would not be significantly affected by external vorticity, so that its development is determined by classical boundary-layer theory with the boundary-layer edge solutions given by the inviscid solution for the surface streamline. Conversely, a relatively thick boundary layer is appreciably influenced by the inviscid shear layer. It was determined that the vortical layer is completely entrained by the boundary layer at a position close to the nose. Thus, over most of the surface, boundary-layer phenomena are governed by the flow emanating from the conical

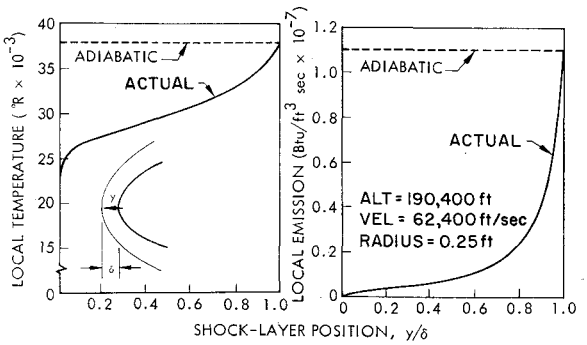

Fig. 10 Influence of cooling on temperature and radiation distribution through the shock layer at the stagnation point.

shock. This effect results in higher effective Reynolds numbers than if the streamlines originated from the stagnation point.

Radiative Heat Transfer

At conditions of interest, the shock layer may be considered optically thin. Thus, if the shock layer is locally approximated as a semi-infinite plane-parallel slab, the radiative heat transfer to the surface is given by integration across the shock layer of the flux emitted per unit volume. At the speeds involved here, radiative cooling of the gas may be appreciable. This effect is illustrated in Fig. 10 for the stagnation point. At the shock, the adiabatic and actual values of temperature and emission rate are identical since the air has had no time to radiate away energy. As the air moves toward the surface it cools, and local emission drops rapidly. For the flight conditions shown, which are typical, the integrated value of the radiation to the surface is about 20% of that which would be calculated assuming adiabatic flow. Approximate, closed-form, analytic solutions[13] that yield results in good agreement with more rigorous techniques[14,15] have been used to evaluate the radiative heating. The nonequilibrium contribution to the total radiation has been estimated and was found to be insignificant for the conditions of interest. Radiation from the wake to the afterbody has been empirically determined.

Thermal Protection

Heat-Shield Material Performance

Considered as requirements for the heat-shield material are fabricability, high heat-absorption capability, good insulation quality, and thermal shock resistance. A state-of-the-art material, nylon-phenolic, was selected. The nylon-phenolic weight ratio is taken as 1:1. The density of the composite is assumed to be 75 lb/ft.[3]

The degradation of nylon-phenolic in the re-entry environment occurs through a complex of processes.[16,17] At elevated temperatures (1000° to 1500° F), the virgin polymers pyrolyze in a reaction layer into high molecular weight gaseous products that leave a solid carbon residue. The carbon char supports high surface temperatures. The pyrolysis gases, during transit through the char to the surface, absorb heat by temperature rise and associated chemical cracking. A theoretical model[16] that rigorously describes the complex physico-chemical processes was used to define the nylon-phenolic performance.

Ablation causes a large reduction in the convective heating; however, radiative heating is not greatly affected. Therefore as radiation fluxes are increased, ablation rates eventually become so large as to move the thermal and diffusion boundary layers off the surface. Under such conditions, material consumption occurs by sublimation.

Heat-shield design

Heat-shield design calculations were performed for a six-man vehicle with a 35° half-cone angle, a W/C_LA value of 340 lb/ft² and $L/D = 0.6$. The initial nose radius was $\frac{1}{4}$ ft. A skip trajectory was assumed that accounted for ablation mass loss. The total heating in such a trajectory is very nearly the same as for the corresponding nonskip trajectory; however, the additional "heat-soak" time makes necessary greater insulation thicknesses. The lower boundary (10-G limit) trajectory was used. The velocity at re-entry is 65,000 fps, and the pull-out altitude is 189,000 ft. Environmental conditions are most severe at the vehicle stagnation point. The total heat transfer is in excess of 1×10^6 Btu/ft². The peak radiative heating rate is 27,000 Btu/ft² sec, and the maximum convective flux is approximately 1% of this value. Radiation cooling of the shock-layer air reduces the peak radiation flux by a factor of about 8 from the adiabatic flow value. Convective heating is reduced to zero during the first 150 sec of re-entry as a consequence of high mass injection rates; it is not until about 200 sec that convective heating becomes appreciable.

Heat-shield material is rapidly consumed during the early portion of re-entry; ablation rates of up to 0.3 in./sec are predicted. When radiation ceases to be significant and convection predominates, material consumption rate is relatively low. The total amount of material ablated is approximately 14 in.

Environmental conditions to which the conical section of the forebody is exposed are somewhat milder than those for the stagnation region. In particular, shock-layer temperatures are lower by a factor of almost 2. As a consequence, radiation heating of the conical surface is considerably less. Shock-layer density on the cone is comparable to that at the stagnation point; the boundary layer is turbulent during the major portion of the heating period. Hence, convection heating rates on the cone are somewhat greater than at the stagnation point. Heat-transfer histories at a representative position on the cone are described in Fig. 11. Although the peak radiative and convective heat fluxes are comparable in magnitude, the heat transferred by convection far exceeds that transferred by the radiative process.

The thermal degradation history of the heat shield at the 10-ft position is also described in Fig. 11. The lower curve shows the surface recession history, whereas the upper curve indicates the depth to which the pyrolysis zone has penetrated. The distance between the two curves is equal to the char-layer thickness. The final extent of degradation is about 3 in. At early times when the ablation rate is high, the char layer is extremely thin. Its thickness is greatest during the early part of the second re-entry period. Additional material is required for insulation of the substructure. A total shield thickness of 3.65 in. on the forebody (apart from the nose

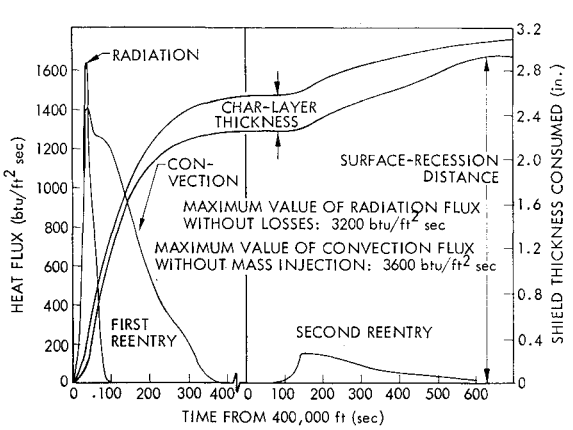

Fig. 11 Heating and ablation histories of cone 10 ft from vehicle tip.

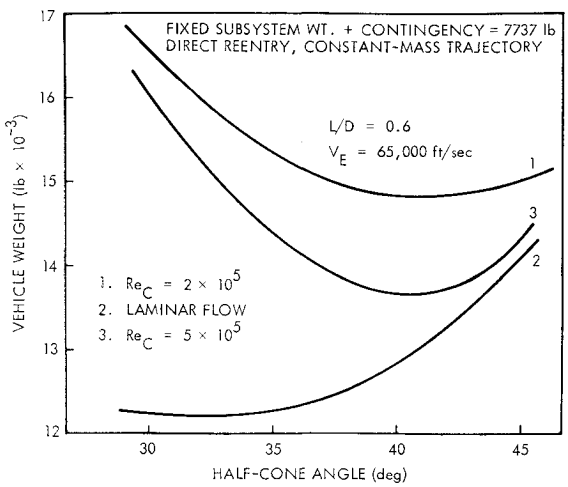

Fig. 12 Variation of vehicle weight with cone angle.

section) insures that the substructure interface temperature does not exceed about 525°F. Thus, attachment of the heat shield to the substructure by a high-temperature plastic bond is possible. Heat transfer to the afterbody section of the vehicle is relatively low, and 1-in. nylon-phenolic is sufficient to limit the substructure temperature rise.

Minimum Weight Configurations

Total heat transfer to the vehicle is a strong function of vehicle geometry. In particular, the influence of cone angle is important (Fig. 12). This effect of bluntness on the total vehicle weight must consider variation in surface area, structural weight factors, and trajectory (due to changes in W/C_LA). A fixed subsystem weight (from subsystem design analyses performed during the study) and the same volume (500 ft^3) and base area (131 ft^2) were used. Constant mass trajectories were used; these yield higher ablator weights than the operational trajectories. The lowest weights are obtained if the boundary layer is laminar; an optimum half-cone angle near 30° is indicated. If the boundary layer is turbulent over most of the vehicle ($Re_C = 2 \times 10^5$), a minimum occurs at about 40°. Generally, increase in weight to the right of the minima is a result of increased radiative heat transfer, whereas increase in weight to the left of the minima reflects larger forecone areas and higher convective heating resulting from the lower pull-out altitude associated with the higher W/C_LA values. Curve 1 of Fig. 12 is considered the more realistic. Total weight at re-entry for a six-man module is about 15,000 lb.

Conclusions

The major conclusions to be drawn from this study are as follows:

1) Basic re-entry criteria can be met with low to moderate L/D characteristics (0.6–1.0).

2) At 65,000 fps, an accuracy of 25 arc-sec or better in approach guidance is required to achieve a reliable re-entry.

3) A closed-loop guidance and navigation system are required for the atmospheric re-entry phase.

4) The proposed configuration adequately meets the requirements of range control, maneuverability, trajectory control, and re-entry corridor width.

5) The compact shape allows maximum use of available space, and the symmetrical flow field permits reliable theoretical analyses.

6) Heat-transfer analyses are strongly influenced by two important uncertainty areas, viz., boundary-layer transition under design conditions and the emissivity of air in the range 15,000° to 40,000°K.

7) The effect of mass transpiration on the boundary layer and radiation loss from the airstream are important mitigating considerations.

8) Ablation heat protection is adequate at speeds up to 65,000 fps; heat-shield weight is approximately one-third of the total vehicle weight.

References

[1] Shapland, D. J. (ed), "Preliminary design of a Mars-mission Earth reentry module," Lockheed Missiles and Space Co., Final Rept., LMSC 4-57-64-1, Contract NAS 9-1702 (February 1964).

[2] Love, E. S., "Factors influencing configuration and performance of multipurpose manned entry vehicles," J. Spacecraft Rockets **1**, 3–12 (1964).

[3] Pritchard, E. B., "Survey of velocity requirements and reentry flight mechanics for manned Mars mission," J. Spacecraft Rockets **1**, 605–610 (1964).

[4] Breakwell, J. V., Helgostam, L. F., and Krop, M. A., "Guidance phenomena for Mars mission," *Advances in the Astronautical Sciences* (Western Periodical Co., Hollywood, Calif., 1963), Vol. 15.

[5] Price, D. A., Kepler, D. I., and Krop, M. A., "Configuration concepts for Earth reentry from planetary missions," Lockheed Missiles and Space Co., LMSC A031360 (May 1963).

[6] Hearne, L. F., Lefferdo, J. M., and Chin, J. H., "Reentry heating and thermal protection of a Mars-mission Earth reentry vehicle," *AIAA Entry Technology Conference* (American Institute of Aeronautics and Astronautics, New York, 1964), pp. 118–135.

[7] Weisner, J. D., private communication, Lockheed Missiles and Space Co., Sunnyvale, Calif. (November 1963).

[8] Nardone, M., Breene, R. G., Zeldin, S., and Riethof, T. R., "Radiance of species in high temperature air," General Electric Co. Space Sciences Lab. Rept. R63SD3 (1963).

[9] Armstrong, B., Buttrey, D., Sartori, L., Siegert, A. J. F., and Weisner, J. D., "Radiative properties of high temperature gases," Lockheed Missiles and Space Co., Air Force Special Weapons Center AFSWC-TR-61-72 (1961).

[10] Hoshizaki, H., "Heat transfer in planetary atmospheres at super-satellite speeds," ARS J. **32**, 1544–1551 (1962).

[11] Lees, L., "Laminar heat transfer over blunt-nosed bodies at hypersonic flight speeds," Jet Propulsion **26**, 259–269 (1956).

[12] Phillips, R. L., "A summary of several techniques used in the analysis of high enthalpy level, high cooling ratio turbulent boundary layers on blunt bodies of revolution," Ramo Wooldridge Corp., GM-TM-194 (1957).

[13] Chin, J. H. and Hearne, L. F., "Shock layer radiation for sphere-cones with radiative decay," Lockheed Missiles and Space Co., LMSC 5-13-64-4 (1964).

[14] Howe, J. T. and Viegas, J. R., "Solutions to the ionized radiating shock layer, including reabsorption and foreign species effects and stagnation region heat transfer," NASA Ames Research Center, TR-R-159 (1963).

[15] Wilson, K. H. and Hoshizaki, H., "Inviscid, nonadiabatic flow about blunt bodies," AIAA Preprint 64-70 (1964).

[16] Kratsch, K. M., Hearne, L. F., and McChesney, H. R., "Theory for the thermophysical performance of charring organic heat shield composite," Lockheed Missiles and Space Co., LMSC 803099 (1963).

[17] Scala, S. M. and Gilbert, L. M., "Thermal degradation of a char-forming plastic during hypersonic flight," ARS J. **32**, 917–924 (1962).